REVISTA TÓPICOS
ISSN 2965-6672 | Qualis A2

ON THE USE OF NASGRO SOFTWARE TO ESTIMATE FATIGUE LIFE UNDER CONSTANT AND VARIABLE AMPLITUDE LOADINGS IN ALUMINUM ALLOY SAE-AMS 7475-T7351

USO DO PROGRAMA NASGRO PARA ESTIMAR VIDA EM FADIGA DE AMPLITUDE CONSTANTE E VARIÁVEL EM LIGAS DE ALUMINIO SAE-AMS 7475-T7351

Engenharias • 20/04/2026

REGISTRO DOI: 10.70773/revistatopicos/776664402

Raimundo Gomes de Amorim Neto[1]

Aline Emanuelle Albuquerque Chemin[2]

Cassius Olivio Figueiredo Terra Ruchert[3]

ABSTRACT

This paper uses several fatigue life prediction models implemented in the NASGRO program to predict crack behavior under constant-amplitude and variable-amplitude loading. The experimental data consist of an aeronautical aluminum alloy SAE-AMS 7475-T7351. C(T) compact specimens were used for constant loading amplitude (CAL), while M(T) specimens were selected for variable load amplitude (VAL). With respect to the constant-amplitude data, the fatigue growth rates, and consequently the parameters of the Paris equation and the KIC values, were obtained from the simulations. In this way, the values obtained were satisfactory, with good correlations. Regarding VAL, the calibration parameters for each interaction model were obtained for each charge spectrum in this work: the TWIST and FALLSTAFF spectra and their mini versions. The NASGRO 4.0 program presented overall good forecasting results.

Keywords: Constant and variable amplitudes; Fatigue life; SAE-AMS 7475-T7351; Aeronautical Aluminum Alloy.

RESUMO

Este artigo utiliza diversos modelos de previsão de vida à fadiga implementados no programa NASGRO para prever o comportamento de trincas sob carregamento de amplitude constante e variável. Os dados experimentais consistem em uma liga de alumínio aeronáutico SAE-AMS 7475-T7351. Corpos de prova compactos C(T) foram utilizados para amplitude de carregamento constante (CAL), enquanto corpos de prova M(T) foram selecionados para amplitude de carregamento variável (VAL). Com relação aos dados de amplitude constante, as taxas de crescimento da fadiga e, consequentemente, os parâmetros da equação de Paris e os valores de KIC foram obtidos a partir das simulações. Dessa forma, os valores obtidos foram satisfatórios, com boas correlações. Em relação à VAL,

os parâmetros de calibração para cada modelo de interação foram obtidos para cada espectro de carga neste trabalho: os espectros TWIST e FALLSTAFF e suas versões mini. O programa NASGRO 4.0 apresentou, de modo geral, bons resultados de previsão.
Palavras-chave: Amplitudes constantes e variáveis; Vida à fadiga; SAE-AMS 7475-T7351; Liga de alumínio aeronáutico.

1. INTRODUCTION

Studying the fatigue crack propagation rate and calculating life under variable-amplitude loading are critical to more reliably predicting the life of structural components. Over the past 30 years, many models have been proposed to predict crack behavior under irregular or random loads [9]. Due to the random nature of variable-amplitude loading [2], it is difficult to model all parameters influencing crack growth under this type of loading. Due to the number and complexity of the mechanisms involved [3] in crack growth retardation, creating a universal model to quantify the interaction effects of loads is quite difficult.

This work aims to compare experimental flight-test results under variable-amplitude loading with numerical responses obtained using fatigue-life prediction programs. The flights in question are military representation, Falstaff and Mini-Falstaff, and civil aviation, Twist and Mini-Twist. On the other hand, it aims to present the fatigue crack growth model in the NASGRO 4.0 software in the non-load interaction mode for constant load amplitudes. To evaluate the performance of the computational simulation to predict the behavior of the real testpieces, by comparing the results with those obtained in [11]. Thus, the parameters of the Paris Equation were used for comparison.

The article is organized as follows: First, experimental results are presented for constant and variable loads. Second, the details of the propagation models used in the study are shown. The numeric results for constant and variable loads are then displayed. Subsequently, the results, the most striking aspects, and, finally, some conclusions are discussed.

2. PROPAGATION MODELS2.1 MODELS OF CONSTANT AMPLITUDE AND CASES OF NON-DEPENDENCY OF LOADING HISTORY

2.1. Models of Constant Amplitude and Cases of Non-dependency of Loading History

In problems where the loads are shown as constant, as well as in the non-consideration of load interaction effects due to the loading history. Paris and Erdogan [1] were the pioneers in proposing a law for crack growth rates, based on experimental data. Several experiments were carried out by measuring the growth rate da/dN as a function of the stress intensity factor. The equation of Paris is given by Equation 1, where C and m are constants dependent on the material.

$$\frac{da}{dN} = C(\Delta K)^m \text{ (Eq. 1)}$$

As the equation presented only the dependence of propagation on ΔK, it inherently cannot represent all problems faithfully, necessitating new models that include the dependence on the load ratio and, thus, the effect of crack closure. One can highlight the equation of form, as presented in Eq. 2.

$$\frac{da}{dN} = \frac{C \cdot \Delta K^m}{(1-R)K_C - \Delta K} \text{(Eq. 2)}$$

Another more robust [10] model was developed by NASA's Forman and Newman, Lockheed Martin's Shivakumar, NLR's Koning, and ESA's Henriksen. The expression is given by Equation 3. For the calculation of fatigue crack growth, the NASGRO equation (Equation 3) was used in this work.

$$\frac{da}{dN} = C[(\frac{1-f}{1-R})\Delta K]^n \frac{(1-\frac{\Delta K_{th}}{\Delta K})^p}{(1-\frac{K_{máx}}{K_C})^q} \text{(Eq. 3)}$$

In this equation, each of the terms has the following meanings: a - crack size; N - number of cycles applied; R - charge ratio; ΔK - variation of the stress intensity factor; ΔKth - lower limit of the variation of the stress intensity factor; Kc - critical stress intensity factor; C, n, p and q - constants derived empirically; F - crack opening function.

2.2. Wheler And Generalized Willenborg Models

The Wheeler model [7] introduced a crack growth rate reduction factor, calculated for each cycle and used as a multiplicative factor in the crack growth increment for that cycle. The empirical delay parameter introduced by Wheeler, Cp, ranges from 0 to 1, and allows a delay by reducing the rate of crack growth after an overload voltage. Wheeler proposed that the exponent m, once calibrated by selecting the value that best approximates experimental curves obtained under a spectrum of loads. The Wheeler model cannot predict the phenomenon of stopping crack growth after a large overload, and it does not consider the effects of underload, that is, delay-reduction effects.

The Willenborg model [3] assumes that the delay in a cycle depends on the loading and the extent of the crack within the plastic

overload zone. Willenborg has assumed that the maximum stress intensity factor, $K_{max,}$ at the current crack length ai will be reduced by a residual-stress factor. K_r. The K_r value is calculated as the difference between the intensity of tension required to produce a zone that could reach the edge of the overload zone, far from the current crack tip, and the current maximum applied stress intensity factor, K_{max}. Willenborg proposed that the two tension-intensity factors, Kmax and Kmin, in the i-th cycle are effectively reduced by a factor of Kr. As the tension factor changes, ΔK remains unchanged due to the uniform reduction, and the delay effect is observed, only by the change in the effective stress ratio, $R_{eff,}$ calculated by Equation 4.

$$R_{eff} = \frac{K_{eff,\min}}{K_{eff,\max}} = \frac{K_{\min} - K_r}{K_{\max} - K_r} \text{(Eq. 4)}$$

As a consequence, crack propagation models that do not explicitly consider the effects of the stress ratio, R, cannot be used with the Willenborg delay model, since the delay effect would not be observed. In addition, this model does not depend on empirical parameters that can be calibrated as with other models, which can generate very imprecise results for different types of charge spectra. According to Schieve [7], a problem in the Willenborg model is the consideration that $K_{eff.\ max} = 0$, i.e., crack arrest, immediately after an overload if $K_{OL} \geq 2K_{max}$. Thus, the model always implies stopping crack growth if the overload-to-subsequent-load ratio exceeds 2, which is not always realistic, because the overload ratio that would imply the stoppage of crack growth depends on several factors, such as material and loading conditions.

Gallagher [3] formulated the Generalized Willenborg model (GW) by introducing an empirical constant into the calculations (Equation 5).

Like the original version, Willenborg's generalized model addresses only delay effects. Gallagher created a relationship between the Willenborg residual stress intensity factor, K_r, and a new stress intensity factor, KRW, so that:

$$K_R^w = \Phi^{K_r} = \left(\frac{1 - \frac{\Delta K_{th}}{\Delta K}}{(R_{SO} - 1)}\right) \cdot K_r \quad \text{(Eq. 5)}$$

According to Meggiolaro [3], typical values for R_{SO} are 3.5 for nickel and steel alloys and 2.3 for aluminum and titanium alloys. Still, these values also depend strongly on the type of charge spectrum applied. According to Harter [6], the typical values of R_{SO} are 3.0 to 2.7 for aluminum alloys, 2.7 for titanium alloys, and 2.0 for steel alloys; calibration of this parameter is required based on the type of loading and material.

2.3. Modified Generalized Willenborg Models

The Modified Generalized Willenborg (MGW) model is a modification of the Generalized Willenborg model proposed by Brussat. [10] To take into account the effect of the reduction of delay caused by compressive loads or even traction underloads. The MGW model, like the GW model, uses a residual stress intensity factor, K_R, which determines the maximum and minimum effective stress intensity factors as follows:

$$\begin{aligned} K_{eff,\max} &= K_{\max} - K_R \\ K_{eff,\min} &= \max\left[(K_{\min} - K_R), 0\right] \qquad K_{\min} > 0 \quad \text{(Eq. 6)} \\ K_{eff,\min} &= K_{\min} \qquad\qquad\qquad K_{\min} \le 0 \end{aligned}$$

To evaluate the reduction in delay effects after underload, the MGW model uses a factor ΦMGW instead of the factor used in the GW model (Equations 7 and 8). This factor, ΦMGW, is defined as a function of the ratio of the $R_{ol} = S_{ul} / S_{ol}$ ratio, where S_{ol} is defined as

the tension caused by the underload after the S_{ul} tension caused by the last overload. The factor Φ_{MGW} is given by equations. 7 and 8. where the factor Φ_0 is the value of Φ_{MGW} for R_{UL} = 0. This factor, Φ0, depends on the material and can be determined experimentally. According to Schijve, all [7] Typical values of Φ_0 vary between 0.2 and 0.8.

$$\Phi_{MGW} = \min\left(1, \frac{2.523\Phi_0}{1 + 3.5(0.25 - R_{UL})^{0,6}}\right) \quad R_{UL} < 0.25 \quad (7)$$

$$\Phi_{MGW} = 1 \quad R_{UL} \geq 0.25 \quad (8)$$

3. EXPERIMENTAL PROCEDURES

3.1. Constant Amplitude Loads

The experimental procedure used the aeronautical grade aluminum alloy SAE-AMS 7475 T7351, testpieces with LT and TL orientations a total of fourteen crack propagation tests were carried out with compact test C(T) under a load of constant amplitude, which sought to cover two types of orientation and also two thicknesses of specimen, to analyze the difference of the stress state behavior, in plane strain (25 mm) and plane stress (2.5 mm). Finally, five loading ratios were used for each set orientation, except for the 25 mm TL case, which used four test pieces, obtaining the da/dN curves as a function of ΔK, following the Standard ASTM 647-18. The experiments, shown in Table 1, were performed on a 250 kN MTS 810 servo-hydraulic machine under load control (R = Kmin/Kmax constant), with a sine wave at frequencies ranging from 8 to 30 Hz, at room temperature.

3.2. Variable Amplitude Loads

For the variable amplitude loads, VAL, M(T) specimens were drawn in the cross direction of the lamination direction, TL, of an AMS 7475-T7351 alloy plate. These specimens were subjected to different loading spectra: for the Twist and Falstaff spectra, two test pieces were tested; for the Twist and Mini-Falstaff spectra, one specimen was tested. For the Falstaff and Mini-Falstaff spectrum, the maximum stress of 200 MPa was used, and for the Twist and Mini-Twist spectrum, the average stress of 80 MPa was used. Two programmed loading spectra were used during this work: the TWIST (Transport Wing Standard), defined by Schijve et al. [4] and the FALSTAFF (Fighter Aircraft Loading Standard for Fatigue) defined by Schijve and Schütz [13], and its reduced versions, mini-twist and Mini-Falstaff, have been widely adopted as a standard spectrum for comparative studies. The GENESIS program was used to generate the loading sequence for each spectrum type: Twist, Falstaff, and their minis.

Table 1. Summary table of constant and variable amplitude tests

Load	Specimen	Thickness (mm)	Laminatio n direction	R	Spectr
Constant	CT	25	LT	0.1	-
				0.3	-
				0.5	-
				0.7	-

of-nasgro-software-to-estimate-fatigue-life-under-constant-and-variable-amplitude-loadings-in-aluminum-alloy-sae-ams-7475-t7351?noblockage

4. NUMERICAL RESULTS

4.1. Constant Amplitude Loads

Fig. 1 (a) and the information in Table 2, for the 25 mm wide specimens and LT orientation, can be seen by comparing the constants of the Paris equations of the simulations and the experimental tests that the error of the constant m is between 8% for R = 0.8 and 4% for R = 0.1. The K_C value correlated well with the ratios R = 0.1, 0.3, 0.7, and 0.8. However, it had a 21% error for the ratio of 0.5. As for constant C, the simulation data were not close to the experimental data, with the lowest error of 13%. This indicates that the simulation curves are shifted left or right relative to the experimental curve on the dN/ΔK graph. But as the values of m are closer, the inclinations between the simulation and the experiments are similar. In general, the overlapping curves for several Rs are consistent, with those due to larger Rs shifted to the left.

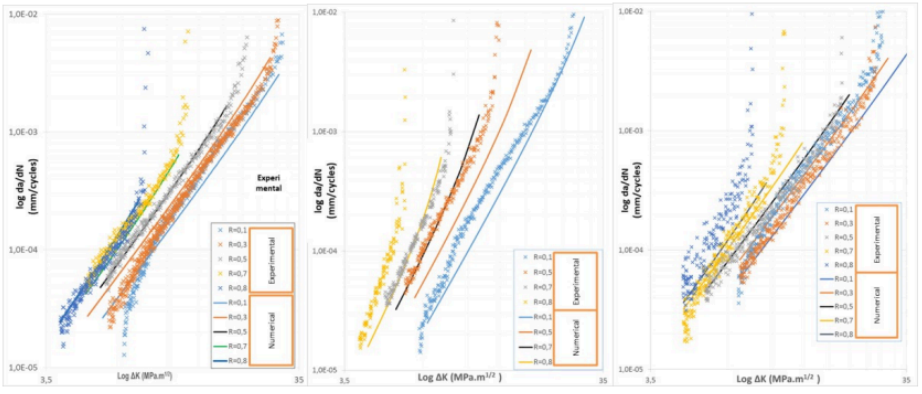

Figure 1. Experimental and numerical response in log da/dN vs log ΔK:
(5) b=25 mm LT. (b) b=25 mm TL and (c) b=2.5 mm LT

Table 2. Experimental and numerical results for the Paris and K-critical constants, for each of the loading ratios in 25 mm wide

specimens, and an LT orientation

Ratio (R)		C	m	Kc (MPa. $m^{1/2}$)
0.1	experimental	1.43E-07	3.02	30.14
	numerical	1.62E-07	2.91	29.15
0.3	experimental	1.43E-07	3.02	28.98
	numerical	2.38E-07	2.91	29.08
0.5	experimental	3.42E-07	2.87	22.03
	numerical	2.60E-07	2.98	18.23
0.7	experimental	3.56E-07	3.05	12.83
	numerical	2.74E-07	3.12	11.47
0.8	experimental	4.21E-07	2.93	8.27
	numerical	3.26E-07	3.18	8.13

Figure 1(b) and the information in Table 3 for the TL test specimens show that the C constant also yielded no results close to the experimental values, with the lowest error of 20% for the body with R = 0.7. This shows a large lateral displacement between the simulated and the experimental curves. The values of m are closer, but the results are relatively farther from the LT test cases, with errors between 3% and 26%. The K_C values were within 9% error for loading ratios 0.1, 0.5, and 0.7, and within 19% error for the load ratio 0.8.

Table 3. Experimental and numerical results for the Paris and K-critical constants, for each of the loading ratios in 25 mm wide specimens, and TL orientation

Ratio (R)		C	m	Kc (MPa. $m^{1/2}$)
0.1	experimental	1.21E-07	4.00	26.92
	numerical	7.14E-08	4.07	29.57
0.5	experimental	2.14E-08	4.33	14.51
	numerical	1.51E-08	4.20	15.02
0.7	experimental	1.02E-08	5.01	9.08
	numerical	1.28E-08	4.56	9.97
0.8	experimental	2.55E-09	6.34	6.00
	numerical	1.01E-09	5.03	7.38

The curves with several overlapping R's are coherent again, showing a close correlation when comparing the distances between the experimental and simulated curves. At this point, the following consideration of material order and preferential grain shape is found in the TL testpieces: the crack is parallel to the preferred direction of the grains, whereas in the LT testpieces, the crack is perpendicular to the preferred direction of the grains. As a result, in LT testpieces, the crack encounters more barriers during its growth, which may indicate an increase in the number of factors not predicted by crack growth simulation software. This shows that the programs do not recognize microstructural problems.

Table 4. Experimental and numerical results for the Paris and K-critical constants, for each of the loading ratios in 2.5 mm wide specimens, and an LT orientation

Ratio (R)		C	m	Kc (MPa. $m^{1/2}$)

0.1	experimental	9.23E-08	3.26	28.57
	numerical	1.72E-07	2.83	27.96
0.3	experimental	1.33E-07	2.99	26.46
	numerical	2.21E-07	2.88	26.48
0.5	experimental	5.76E-07	2.54	19.59
	numerical	2.93E-07	2.88	19.78
0.7	experimental	1.55E-07	3.38	11.49
	numerical	3.31E-07	2.95	12.69
0.8	experimental	1.37E-07	3.77	8.73
	numerical	3.21E-07	3.05	9.25

The specimens with 2.5 mm thickness and LT orientation showed the greatest differences in the constant C values. However, the K_C values were the closest to the experimental results. The values of the constant m had errors ranging from 3% to 23%, with 3 specimens close to 15%. These results are illustrated by Tab. 4 and Fig. 1(c). This higher correlation between the simulations and the actual experiments can be explained by the fact that the computational models for fatigue crack growth are more closely aligned with the plain-stress conditions present in thinner specimens.

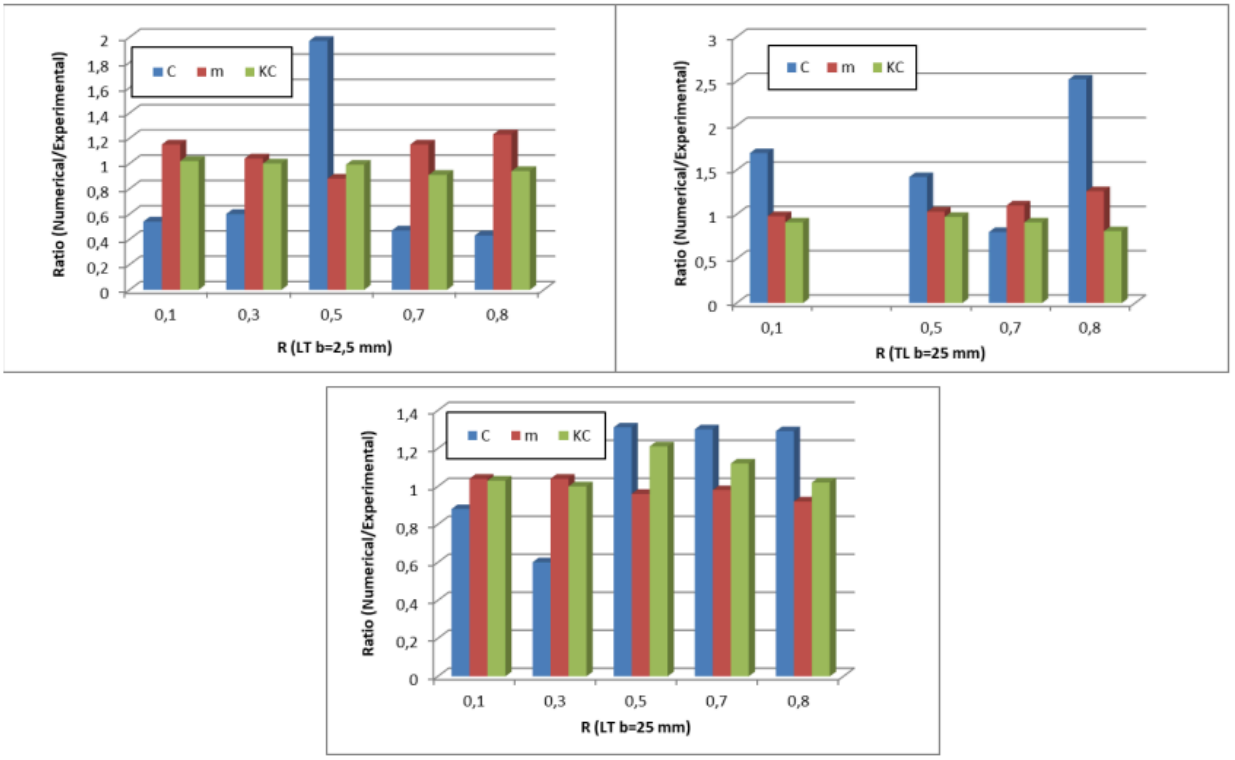

Figure 2. Relations between experimental and numerical quantities: (a) b=25 mm LT, (b) b=25 mm TL e (c) b=2.5 mm LT orientations.

The overlapping curves with several R values are consistent with the curves shifting leftward as R increases. In theory, the same material should have the value of the constant m equal to different values of the loading ratio R. Thus, the specimens in the LT direction presented a smaller deviation from the values of m, with a smaller deviation (0.08) for the thickness of 2.5 mm (0.12 for b = 25 mm LT). The TL test specimens showed a greater deviation of about 0.50. Table 7 summarizes all the values of the experiment/simulation ratios. In general, there is a better correlation between the experimental and simulated values in the constant "m" and "K_C". In the constant "C", the largest difference between the experimental and simulated values was for the testpiece with R = 0.8 and TL orientation, due to the high state of stress, with the experiment/simulation ratio being 2.52.

4.2. Variable Amplitude Loads

For the VAL obtained from the modeling, each flight spectrum is presented sequentially. In all cases, the results were also considered without accounting for load interaction effects, in addition to using the various interaction models, whose delay parameters were calibrated for each type of charge spectrum to minimize the difference between the numerical and experimental responses. As a rule, the calibration parameters were adopted for each interaction model when the result was more conservative, although sometimes the resulting parameter yielded smaller errors in the relative response.

Table 5. Life in number of flights for the spectrums Mini-Twist and Twist.

Mini-Twist	**No. of Flights**		**Twist**	**No. of Flights**
Without retardation	4239		Without retardation	2458
GW (R_{SO} = 2.3)	7976		GW (R_{SO} = 3.9)	2809
MGW (Φ_0 = 0.8)	7529		MGW (Φ_0 = 0.4)	2748
Test 1	9370		Test 1	2936
Test 2	9098		-	-

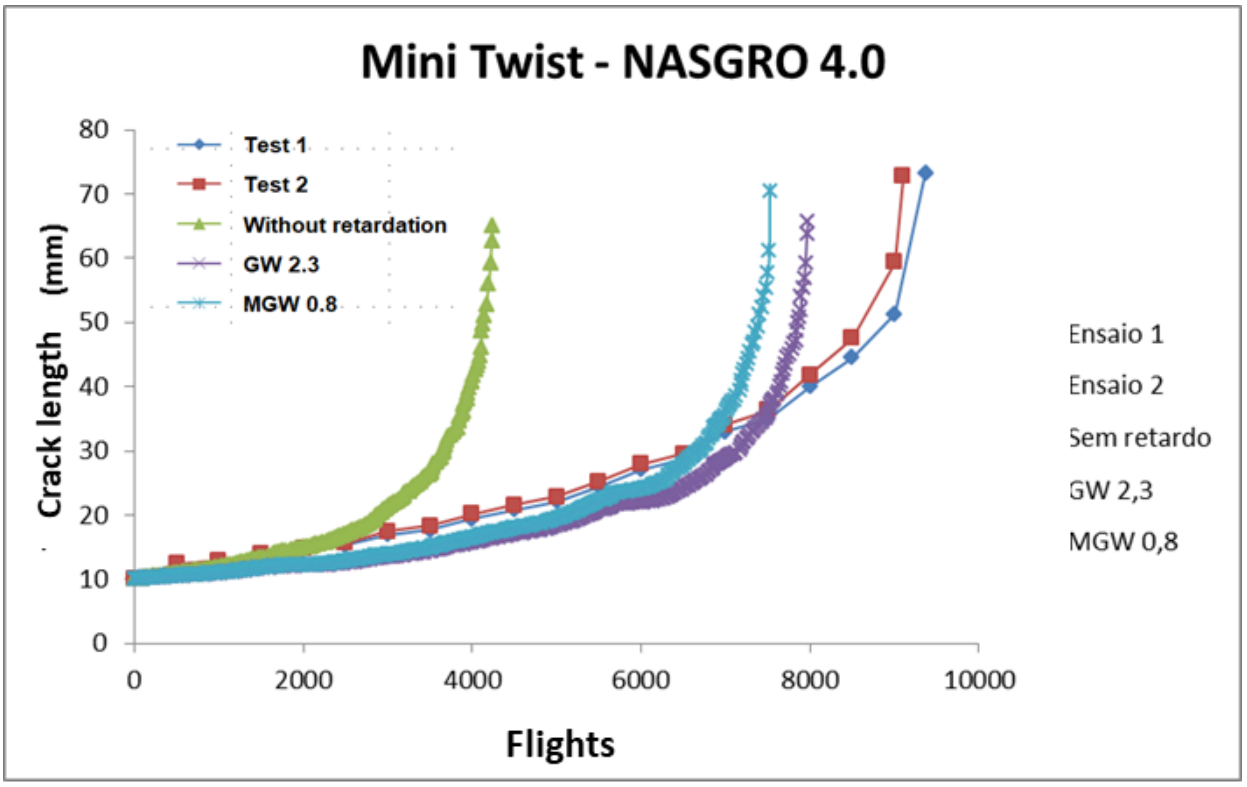

Figure 3. Propagation Curves for spectrums: (a) Mini-Twist and (b)Twist.

Table 5 shows the results for the Twist and Mini-Twist spectra. In turn, Figure 3 illustrates the crack's behavior throughout its life for the experiments and modeling. In the case of the Mini-Twist spectrum, the following values were obtained from calibrating the response to the delay-model parameters: R_{SO} = 2.3 and Φ0 = 0.8 for the Generalized Willenborg (GW) and Modified Generalized Willenborg (MGW), respectively. Table 5 and Figure 3(b) present the results for the Twist-type loading spectrum. In this case, the following values were obtained by calibrating the response to the delay-model parameters: R_{SO} = 3.9 and Φ0 = 0.4 for the Generalized Willenborg (GW) and Modified Generalized Willenborg (MGW) models, respectively.

Table 6 and Figure 4 (a) show the results for the Mini-Falstaff loading spectrum. In this case, the following values were obtained by calibrating the response to the delay-model parameters: RSO = 2.3 and Φ0 = 0.9 for the Generalized Willenborg (GW) and Modified Generalized Willenborg (MGW) models, respectively.

Table 6. Life in number of flights for the spectrums Mini-Falstaff and Falstaff.

Mini-Twist	**No. of Flights**		**Twist**	**No. of Flights**
Without retardation	1393		Without retardation	1425
GW (R_{SO} = 2.3)	4773		GW (R_{SO} = 2.7)	3597
MGW (Φ_0 = 0.9)	4913		MGW (Φ_0 = 0.7)	3744
Test 1	5330		Test 1	5572
			Test 2	4088

Table 6 and Figure 4 (b) present the results for the Falstaff loading spectrum. The table shows the life results for each model. In the case of the Falstaff spectrum, the following values were obtained by calibrating the response to the delay-model parameters: RSO = 2.7 and Φ0 = 0.7 for the Generalized Willenborg (GW) and Modified Generalized Willenborg (MGW) models, respectively. For models with no interaction caused by the delay, the numerical response again diverges significantly from the experimental response, a fact amplified by the difference between the experimental responses, since the two tests differ in a representative way, as expected.

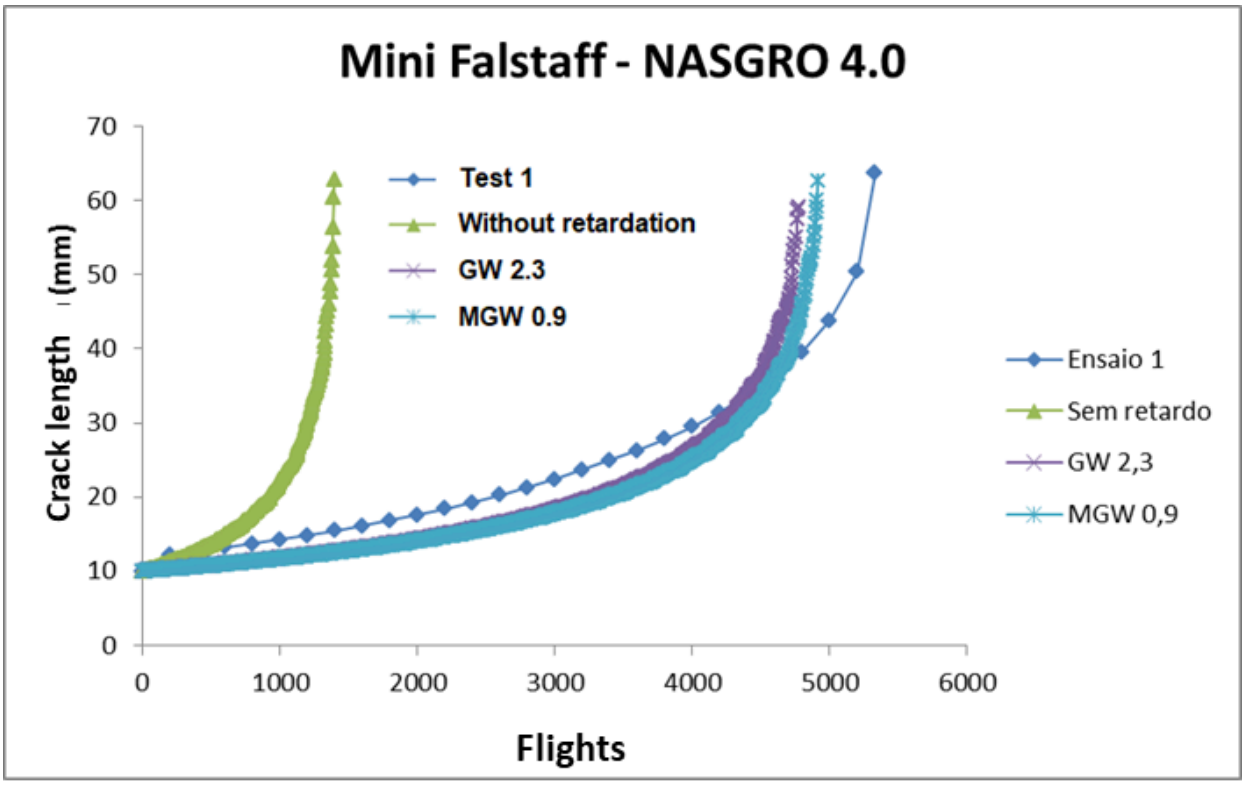

Figure 4. Propagation Curves for spectrums: (a) Mini-Falstaff and (b) Falstaff.

5. CONCLUSIONS

Disregarding the effects of load interaction can lead to results that differ considerably from the actual ones. Among all cases, the best predictions were obtained for the Twist spectrum. This fact possibly indicates that, due to the large number of cycles present in the Twist spectrum, it is not a very random and severe spectrum compared to Falstaff, thus the effects of overloads and consequently of delay have less influence on the result of life in fatigue. For the Twist and Mini-Twist loading spectrum, the MGW model, the only one that accounts for the effects of underload (i.e., delay reduction), showed a lower life than the GW model. This indicates that for these types of loading spectra, the underload can significantly influence life predictions. For the Falstaff and Mini-Falstaff loading spectrum, where MGW model results indicate longer lives than the GW models, which possibly indicates that less severe loads have a lower influence on fatigue life, as already modeled without load interaction.

References

1. Anderson. T. L. Fracture Mechanics: Fundamentals and Applications. 3ª. Boca Raton: Taylor & Francis Group. 2005.

2. Beden. S. M. Abdullah. S. Ariffin. A. K. Al-Asady. N. A. “Fatigue crack growth simulation of aluminum alloy under spectrum loadings”. Materials and Design. Vol. 31. No. 7. pp. 3449-3456. August (2010).

3. Castro. J. P. P. Meggiolaro. M. A. “Comparing overload-induced retardation models on fatigue crack propagation”. 56° Congresso Anual da ABM. Belo Horizonte. MG. Julho (2001).

4. Jonge. J. B. Schütz. D. Lowak. H. Schijve. J. “A Standardized Load Sequence for Flight Simulation Tests on Transport Aircraft Wing Structures”. NLR TR 73029 U. (1973).

5. Forman. R.G. S.R Mettu. S.R. “Behavior of surface and corner cracks subjected to tensile and bending loads in Ti-6Al-4V alloy”. Fracture Mechanics 22nd Symposium. Vol. 1. ASTM STP 1131. H.A. Saxena and D.L. McDowell. eds. American Society for Testing and Materials. Philadelphia. 1992.

6. Harter. J. A. “AFGROW Version 4.0012.15 Users Guide and Technical Manual”. AFRL-VA-WP-TR-2008-XXXX. Air Force Research Laboratory. Ohio. July (2008).

7. Khan. S. U. Alderliesten. R. C. Schijve. J. Benedictus. R., “On the fatigue crack growth prediction under variable amplitude loading”. Computational & Experimental Analysis of Damaged

Materials. Transworld Research Network. Kerala. India. pp. 77-105. (2007).

8. Moreno. B. Martin. A. Lopez-Crespo. P. Zapatero. J., & Domínguez. J. (2015). On the use of NASGRO software to estimate fatigue crack growth under variable amplitude loading in aluminum alloy 2024-T351. Procedia Engineering. 101. 302-311.

9. NASA Johnson Space; Southwest Research Institute. NASGRO 4.0 Fracture Mechanics and Fatigue Crack Growth Analysis Software - Reference Manual. San Antonio. TX: Southwest Research Institute. 2002.

10. NASGRO 4.0 – “Fracture Mechanics and Fatigue Crack Growth Analysis Software”. Reference Manual. Southwest Research Institute. San Antonio. Texas. May (2002).

11. Ruchert. C. O. F. T. “Estudo da Interferência de Carregamento em Histórias de Voos Simulados na Liga de Al Aeronáutico SAE – AMS 7475 T7351”. Tese de Doutorado - Universidade de São Paulo. Escola de Engenharia de São Carlos. pp. 176-191. (2007).

12. Schijve. J. Vlutters. A. M. Ichsan. e Provó Kluit. J. C. “Crack Growth in Aluminum Alloy Sheet Material under Flight-Simulation Loading”. International Journal of Fatigue 7. No.3. pp. 127-136. (1984).

13. Van Dijk. G. M. de Jonge. J. B. Lowak. H. Schütz. D. et al. “FALSTAFF: A description of a Fighter Aircraft Loading Standard for Fatigue evaluation”. Joint publication by F+W

(Switzerland). LBF, IABG (Germany), and NLR (The Netherlands). (1976).

---

[1] Universidade Federal Rural do Semi-Árido, Campus Leste, Centro de Engenharias. Av. Francisco Mota, 572 - Bairro Costa e Silva, Mossoró/RN/Brazil. E-mail: raimundoamorim@ufersa.edu.br

[2] University of São Paulo - Escola de Engenharia de Lorena - Polo-Urbo Industrial, Gleba AI-6, s/n° - CAMPUS II, Lorena/SP/Brazil. E-mail: aline.albuquerque@usp.br

[3] University of São Paulo - Escola de Engenharia de Lorena - Av. João Dagnone, 1100, Jd. Sta Angelina, São Carlos/SP/Brazil. E-mail: cassiusterra@usp.br